Experimental Validation of the Dissociation Hypothesis for Single Bubble Sonoluminescence

Jeffrey A. Ketterling and Robert E. Apfel
Department of Mechanical Engineering, Yale University, New Haven, Connecticut 06520
(Received 14 August 1998)

Single bubble sonoluminescence stability in ambient radius (R_0), drive pressure (P_a) phase space is examined for water partially saturated with pure argon, pure nitrogen, and argon/nitrogen mixtures in order to examine the dissociation hypothesis (DH) of Lohse and Hilgenfeldt [J. Chem. Phys. **107**, 6986 (1997)]. A stroboscopic imaging system was employed to measure R_0 and the maximum bubble radius $R_{\max}$. P_a was calculated by fitting the Rayleigh-Plesset equation to R_0 and $R_{\max}$. Excellent agreement was seen between experiment and prediction over a wide range of parameters, validating DH. [S0031-9007(98)07715-1]

PACS numbers: 78.60.Mq, 43.25.+y

A single bubble trapped in a sound field can be driven into nonlinear radial oscillations when the acoustic drive pressure P_a is sufficiently high. When the collapse is violent enough, the bubble can emit a pulse of light at each acoustic cycle [1]. This phenomenon has been labeled single bubble sonoluminescence (SBSL). Since its discovery, the dependence of SBSL on experimental parameters has been thoroughly examined [2].

One of the significant early observations of SBSL was that the intensity of light emission was dependent on the presence of noble gases [3]. An analysis by Löfstedt *et al.* [4] revealed that, when the drive pressures were in the SBSL regime and mixtures of nitrogen and a noble gas were used, the measured physical parameters of the bubble were not consistent with a diffusive stability picture of bubble dynamics. This led the authors to hypothesize that an "anomalous mass flow mechanism" must be present.

Hilgenfeldt *et al.* [5] then proposed that this unidentified mechanism was chemical in nature. Using a detailed analysis of bubble stability in the R_0-P_a phase space, it was proposed that this chemical process was the dissociation of the diatomic gases into chemical species that then diffused out of the bubble [6,7]. For a bubble composed of argon and nitrogen, the basic idea is that for very low P_a the bubble responds as if it contained both gases inside of it. In the R_0-P_a phase space, a stable bubble will tend to dissolve because the diffusive equilibrium for the total gas saturation is unstable. Subsequently, as P_a increases, the bubble begins a "dancing" motion as it repeatedly undergoes a growth and breakup [1,8,9]. Eventually, the temperature inside the bubble is sufficiently high to dissociate the nitrogen, and a chemical equilibrium is reached where the amount of nitrogen entering the bubble during each cycle is equal to the amount being burned off. In the R_0-P_a phase space the bubble will lie near a negatively sloped curve representing the *stable* chemical equilibrium. As P_a is further increased, the nitrogen in the bubble completely burns off, leaving a bubble with only argon. Now, in the R_0-P_a phase space, the bubble will lie on a positively sloped *stable* diffusive equilibrium curve representing the argon concentration. In other words, when the bubble luminesces, it is the argon concentration that determines stability in the phase space.

A great deal of evidence has been gathered from the literature to support this theoretical picture of SBSL [5–7] which we shall refer to as the "dissociation hypothesis" (DH). In particular, Gaitan and Holt [10] showed that, for water partially saturated with air, the effective gas concentrations for non-SL stable bubbles agreed with a family of diffusive equilibrium curves of decreasing concentrations. A line drawn through the points would have a negative slope in the R_0-P_a phase space. When the bubble reached stable SL, the effective gas concentration computed for each data point agreed with a single stable diffusive equilibrium curve that was 2 orders of magnitude less than the total gas saturation. These findings, along with the data presented in P_a-R_0 phase diagrams [8], provide very strong evidence for DH. Strong evidence for DH was also seen in the non-steady-state experiments of Matula and Crum [11]. Barber *et al.* [12] also show a phase diagram for one argon/nitrogen mixture and one pure argon case. However, no experiments have yet been performed with the specific intent of examining the steady-state predictions of DH.

We present experimental phase diagrams for pure argon, pure nitrogen, and mixtures of argon and nitrogen, and directly compare them to the steady-state predictions of DH. Our intent is to show that, when the bubble is stable and luminescing, it lies on a positively sloped equilibrium curve in R_0-P_a space, representing diffusive stability for the concentration of argon in the fluid regardless of how much nitrogen is present. This is one of the fundamental assumptions of DH but, as of yet, it has not been thoroughly probed experimentally.

The experimental apparatus was a sealed, water-filled cylindrical quartz crystal cell (76 mm diameter, 74 mm height) with brass end caps. The cell was operated at 33.4 kHz which corresponded to the ($r = 2$, $\theta = 0$, $z = 2$) mode. The upper brass end cap contained a thermocouple to measure fluid temperature and a removable

0.25 inch diameter brass plug. The plug was removed just prior to beginning an experiment, resulting in a tiny pressure release surface that was necessary to obtain a resonant mode that could predictably trap a bubble. A small amount of air could thus diffuse into the cell, but the effect on the experimental results was minimal. The opening also permitted a syringe needle to be inserted into the cell, allowing a bubble to be seeded from the gas trapped on the needle tip. A small piezoelectric pill transducer was bonded with epoxy to the upper brass end cap to locate the resonant frequency of the cell. A nominal P_a was found by calibrating the pill transducer against a custom-made hydrophone inserted into the cell.

A vacuum flask containing room temperature distilled, filtered water was connected to the cell via two fluid lines. The vacuum flask was also connected to an automated gas handling system. This system degassed the water, mixed together the desired ratio of argon and nitrogen, and then saturated that mixture into the degassed water to the desired concentration. The gas saturation was inferred using Henry's law. The combined absolute pressure of the argon and nitrogen mixture was $\approx$200 pounds per square inch (psi) with a $\pm$0.5 psi error for each gas component. Because of limitations in measuring the water temperature during gas saturation, it was known only to within ± 1 °C, making it difficult to achieve saturations below the corresponding change in vapor pressure of $\approx$1 Torr. Once the fluid was prepared, it was transferred to the cell (still under a partial vacuum) via the two fluid lines using gravity flow and then brought to atmospheric pressure. Up to that point, the fluid was not exposed to any air or to any pressure above what the fluid was saturated to.

The cell was then placed in a bracket that held it fixed relative to several diagnostic tools and the plug was removed from the upper end cap. The diagnostic tools consisted of a photomultiplier tube (PMT) to measure the relative intensity of the light pulse, a He-Ne laser and PMT to perform light scattering measurements, and a stroboscopic imaging system (SIS). The SIS was essentially that described in Ref. [13] with two alterations. The first was small glass windows attached with silicone sealant to the side of the cell in the path of the light-emitting diode and microscope. The space between the window and the cell was filled with water, helping to correct for the astigmatism caused by the curvature of the cell wall. The second was a digital charge-coupled device (Pulnix TM-9701), the output of which could be sent to computer random-access memory in real time. This allowed movies of the bubble oscillation to be captured and analyzed in near real time to obtain a time averaged radius-time $R(t)$ history of the bubble. Figure 1 shows a typical result of the video analysis. A digital trigger was designed so that video acquisition always commenced on the same point of the drive signal.

From the $R(t)$ curve, two key parameters were extracted: the maximum radius $R_{\max}$ (± 1.1 μm) and R_0 (± 0.9 μm). The radius error values represent the experimental precision and reflect the uncertainty of the pixel value used to threshold the bubble image before edge detecting. We define R_0 as the bubble radius when the ambient pressure is 1 atm. Figure 1 shows where, in relation to the drive signal, R_0 was obtained on the $R(t)$ curve. This method of finding R_0 was possible because, after the bubble collapses and begins to grow, its radius adjusts to the outside pressure to maintain a quasistatic equilibrium size [14]. This also corresponds to the definition of R_0 in the Rayleigh-Plesset (RP) equation. The particular form of the equation we used, details of which can be found in Ref. [7], contained a polytropic exponent and a van der Waals hard core term to describe the gas pressure in the bubble. We used the RP equation to determine P_a (± 0.07 bar) by fitting it to $R_{\max}$ and R_0. The standard room temperature material constants were used for the remaining parameters of the RP equation. The P_a found that using this method was more reliable than the pill transducer calibration and was the method used for all of the data presented in this Letter.

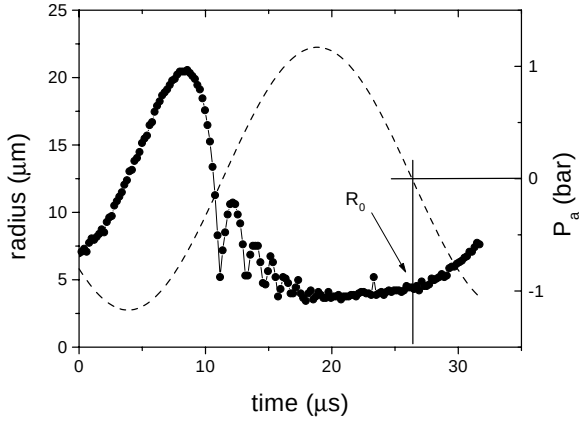

FIG. 1. $R(t)$ curve (circles) found using SIS. P_a was 1.23 bar and the bubble was not luminescing. Each point represents one frame of video. $P_a(t)$ (dashed line) is also shown with the proper phase relation to $R(t)$. The point on the $R(t)$ curve used to determine R_0 is indicated to be where $P_a(t)$ crosses zero on its falling edge. Since the bubble radius responds to the external pressure in a quasistatic fashion, this point represents the radius when the external pressure is 1 atm (ambient pressure), which is the definition of R_0.

After collecting data for a series of P_a with the SIS and analyzing the results, a phase diagram could be mapped out. Figure 2 shows a phase diagram using air saturated in water to 20% [15]. Each data point represents data from a single $R(t)$ curve and is indicated to be luminescing and/or stable. The curves shown in the plot represent diffusive equilibrium curves for a fixed gas concentration (C) computed at 33.4 kHz using the Eller-Flynn formulation [16]. A positive slope represents diffusive stability while a negative slope represents an unstable diffusive equilibrium. Bubbles to the right of a curve tend to grow by rectified diffusion [4,7,16] while bubbles to the left tend to dissolve.

The behavior of the bubble with increasing P_a is similar to what has been reported by other groups [1,8,9]. At low P_a ($<$1.0 bar) the bubble tends to dissolve within a few

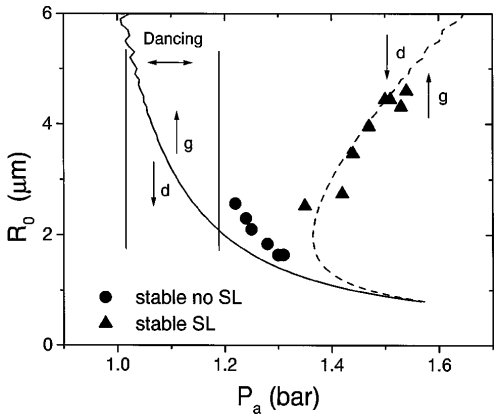

FIG. 2. Phase diagram for air saturated in water to 20% yielding a final argon concentration of 0.2%. Each data point represents the P_a and R_0 found from a single $R(t)$ curve and is indicated to be luminescing and/or stable. The curves in the plot are lines of diffusive equilibrium for a given gas concentration $C = 20\%$ (solid line) and $C = 0.2\%$ (dashed line). The range of P_a where dancing was observed is indicated as are regions of bubble growth (g) and dissolution (d) relative to each equilibrium curve. The stable no SL points (circles) correspond to a *stable* chemical equilibrium which would lie above the $C = 20\%$ curve if plotted.

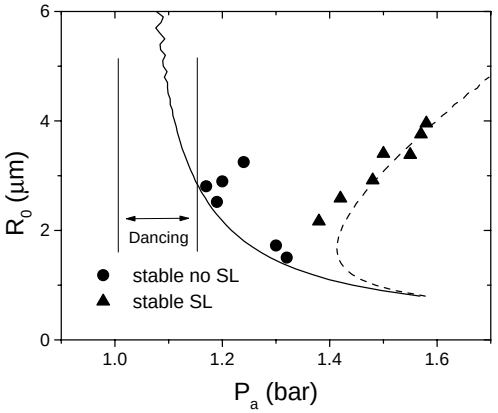

FIG. 3. Phase diagram for a mixture of 1% argon and 99% nitrogen saturated to 10%, yielding a final argon concentration of 0.1%. The diffusive equilibrium curves are for $C = 10\%$ (solid line) and $C = 0.1\%$ (dashed line).

seconds. As P_a is increased, the bubble begins dancing until it becomes stable at $P_a \approx 1.2$ bar. With a further increase in P_a the bubble remains stable, decreases in ambient radius, and the points can be described by a negatively sloped curve representing the *stable* chemical equilibrium. This equilibrium acts to "bridge" the growth region to the right of the $C = 20\%$ curve and the dissolution region to the left of the $C = 0.2\%$ curve [7]. Near $P_a \approx 1.35$ bar the bubble begins to luminesce and grows in R_0 until the upper threshold of $P_a \approx 1.55$ bar. When the bubble is luminescing, it lies near the *stable* diffusive equilibrium curve corresponding to the argon concentration of 0.2%.

The above results can be compared to "artificial" air consisting of 1% argon and 99% nitrogen at 10% saturation (Fig. 3). The final argon concentration is now 0.1% instead of 0.2% as in the above case. The general behavior in phase space is the same as in Fig. 2, except for one major difference. The stable SL points now lie near the $C = 0.1\%$ *stable* diffusive equilibrium curve which is consistent with the amount of argon saturated in the fluid. The clear shift in the location of the stable SL in phase space as the argon concentration changes is exactly what DH predicts.

By saturating the pure form of each gas into the fluid separately, their individual effect on the phase space diagram can be isolated. Figure 4 shows a case with nitrogen saturated to 10%. In this case no stable or unstable SL was seen, confirming the observation that noble gases are needed to obtain stable SL [3]. Just as before, the stable non-SL points appear to fall on a negatively sloped curve corresponding to the *stable* chemical equilibrium. We should note that, without careful preparation of the fluid or when pure nitrogen was saturated above 20%, a region of very unstable weak SL was observed, as reported by Hiller *et al.* [3].

Figure 5 shows a phase diagram for pure argon saturated to 0.26%. In this case, only stable SL is seen and the points fall on the *stable* diffusive equilibrium curve corresponding to the argon partial pressure. Near $P_a \approx 1.5$ bar a small region of unstable SL was observed as the bubble most likely approached the shape stability threshold [5,8]. The phase diagrams of Figs. 4 and 5 both agree with the steady-state predictions of DH and confirm that it is the argon that determines the stable SL branch of the diagram and that the nitrogen determines the stable non-SL branch.

In summary, the results presented here provide compelling evidence for DH. Phase diagrams have been mapped out for numerous other argon/nitrogen mixtures and saturations, and the results are all similar to the results presented in this Letter up to total saturations of ≈50%. Above this saturation, the behavior of the bubble in phase space did not appear to fit a predictable pattern, very likely due to the bubble being unable to burn off enough nitrogen during

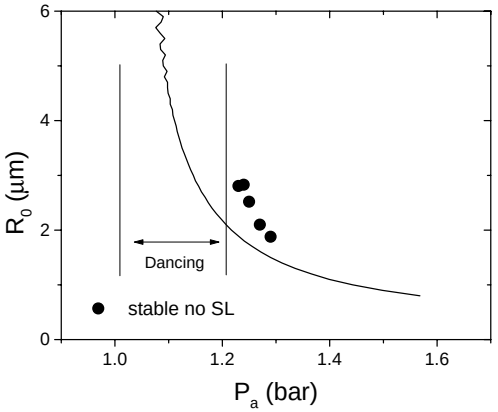

FIG. 4. Phase diagram for pure nitrogen saturated to 10%. The diffusive equilibrium curve is for $C = 10\%$ (solid line). With no argon present, no SL was observed. Above $P_a \approx 1.3$ bar, the bubble dissolved.

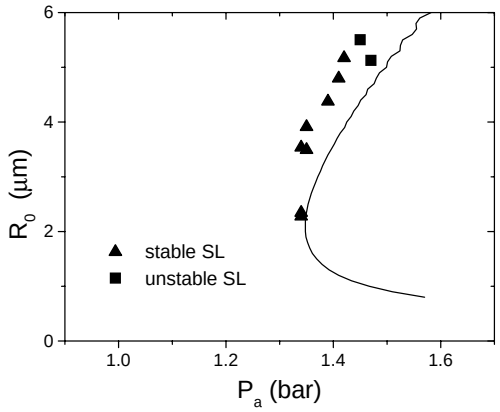

FIG. 5. Phase diagram for pure argon saturated to 0.26%. The diffusive equilibrium curve is for $C = 0.26\%$ (solid line). With only argon present, only stable SL was observed. No bubble (stable or unstable) could be trapped below $P_a \approx$ 1.3 bar and no dancing was observed.

each cycle to ever reach a stable equilibrium; thus even when it is luminescing, it still has some nitrogen present. This may be why very weak unstable SL was observed when using pure nitrogen at above ≈20% saturation.

The incomplete nitrogen burnoff may also be why we observed a difference in maximum light intensity between pure argon and argon/nitrogen mixtures when the argon concentration was held constant. The maximum light intensity of pure argon was noticeably less than that of argon/nitrogen mixtures as was reported in Ref. [3]. Small changes in the expansion ratio ($R_{\max}/R_0$) have been shown experimentally [9,17] and theoretically [18] to have a large effect on light emission so the difference may be due to subtle differences in bubble dynamics. The theoretical results of Vuong and Szeri [19], showing that pure noble gas bubbles do not shock as strongly as air-filled bubbles, may also be relevant to the observed differences in light intensity. Possibly with a more rigorous treatment of the gas over each cycle, including chemical, thermal, and diffusive effects such as being pursued by Szeri and Storey [20], these subtle divergences from DH could be accounted for.

Another novel implication of the results is that the concentration of an inert gas can be inferred from an unknown gas mixture if a stable region of SL is observed.

We wish to thank R. Holt, T. Matula, and R. Roy for many valuable discussions. We also wish to thank Y. Tian and J. Jankovsky for their assistance in constructing the experimental apparatus.

[1] D. F. Gaitan, Ph.D. dissertation, University of Mississippi, 1990; D. F. Gaitan *et al.,* J. Acoust. Soc. Am. **91**, 3166 (1992).
[2] B. P. Barber *et al.* [Phys. Rep. **281**, 65 (1997)] provides a thorough review of experimental results, particularly those of Putterman's UCLA group.
[3] R. Hiller *et al.,* Science **266**, 248 (1994).
[4] R. Löfstedt *et al.,* Phys. Rev. E **51**, 4400 (1995).
[5] S. Hilgenfeldt, D. Lohse, and M. P. Brenner, Phys. Fluids **8**, 2808 (1996).
[6] D. Lohse *et al.,* Phys. Rev. Lett. **78**, 1359 (1997).
[7] D. Lohse and S. Hilgenfeldt, J. Chem. Phys. **107**, 6986 (1997).
[8] R. G. Holt and D. F. Gaitan, Phys. Rev. Lett. **77**, 3791 (1996).
[9] B. P. Barber *et al.,* Phys. Rev. Lett. **72**, 1380 (1994).
[10] D. F. Gaitan and R. G. Holt, in *Proceedings of the 16th International Congress of Acoustics and the 135th Meeting of the Acoustic Society of America, Seattle,* edited by P. Kuhl and L. Crum (ASA, New York, 1998), p. 2569.
[11] T. J. Matula and L. A. Crum, Phys. Rev. Lett. **80**, 865 (1998).
[12] Barber *et al.* (Ref. [2]), Fig. 43.
[13] Y. Tian, J. A. Ketterling, and R. E. Apfel, J. Acoust. Soc. Am. **100**, 3976 (1996).
[14] F. G. Blake, *Technical Memorandum No. 12* (Harvard Acoustics Research Laboratory, Cambridge, MA, 1949).
[15] Holt and Gaitan (Ref. [8]) [Fig. 1(c)] examine the same case but at 20.8 kHz.
[16] A. Eller and H. G. Flynn, J. Acoust. Soc. Am. **37**, 493 (1965); M. M. Fyrillas and A. J. Szeri, J. Fluid Mech. **277**, 381 (1994).
[17] D. F. Gaitan and R. G. Holt (to be published).
[18] L. Kondić, J. I. Gersten, and C. Yuan, Phys. Rev. E **52**, 4976 (1995); W. C. Moss, D. B. Clarke, and D. A. Young, Science **276**, 1398 (1997).
[19] V. Q. Vuong and A. J. Szeri, Phys. Fluids **8**, 2354 (1996).
[20] A. Szeri and B. Storey, J. Acoust. Soc. Am. **103**, 3076 (1998).